Ultrafast Shock Compression of Self-Assembled Monolayers: A Molecular Picture

James E. Patterson[†] and Dana D. Dlott*

School of Chemical Sciences, University of Illinois at Urbana–Champaign, Box 01-6 CLSL, 600 South Mathews Avenue, Urbana, Illinois 61801

Simulations of self-assembled monolayers (SAMs) are performed to interpret experimental measurements of ultrafast ∼1 GPa (volume compression $\Delta V \sim 0.1$) planar shock compression dynamics probed by vibrational sum-frequency generation (SFG) spectroscopy (Lagutchev, A. S.; Patterson, J. E.; Huang, W.; Dlott, D. D. *J. Phys. Chem. B* **2005,** *109,* XXXX). The SAMs investigated are octadecanethiol (ODT) and pentadecanethiol (PDT) on Au(111) and Ag(111) substrates, and benzyl mercaptan (BMT) on Au(111). In the alkane SAMs, SFG is sensitive to the instantaneous orientation of the terminal methyl; in BMT it is sensitive to the phenyl orientation. Computed structures of alkane SAMs are in good agreement with experiment. In alkanes, the energies of gauche defects increase with increasing number and depth below the methyl plane, with the exception of ODT/Au where both single and double gauche defects at the two uppermost dihedrals have similar energies. Simulations of isothermal uniaxial compression of SAM lattices show that chain and methyl tilting is predominant in PDT/Au, ODT/Ag and PDT/Ag, whereas single and double gauche defect formation is predominant in ODT/Au. Time-resolved shock data showing transient SFG signal loss of ODT/Au and PDT/Au are fit by calculations of the terminal group orientations as a function of ΔV and their contributions to the SFG hyperpolarizability. The highly elastic response of PDT/Au results from shock-generated methyl and chain tilting. The viscoelastic response of ODT/Au results from shock generation of single and double gauche defects. Isothermal compression simulations help explain and fit the time dependence of shock spectra but generally underestimate the magnitude of SFG signal loss because they do not include effects of high-strain-rate dynamics and shock front and surface irregularities.

1. Introduction

In the previous paper,[1] experimental measurements were reported of ultrafast ∼1 GPa shock compression of self-assembled monolayers (SAMs) on evaporated polycrystalline Au or Ag (111) substrates, using vibrational sum-frequency generation (SFG) spectroscopy[2−4] in the C−H stretching region as a probe of the instantaneous orientation of the terminal functional group.[1,5,6] The dynamic reorientation of the SAM terminus serves as a measure of monolayer elasticity and viscoelasticity under conditions of fast, large-amplitude uniaxial compression.[1,6−9] In this paper we describe work that was done to model these experiments. Using molecular mechanics methods we determine the relative stabilities of various molecular conformers under conditions of uniaxial compression. The orientations of the terminal groups of these conformers are determined and used to compute a molecular hyperpolarizability that can be compared to the shock spectroscopy measurements.

The shock spectroscopy technique provides a real-time probe of the behavior of ordered oriented interfacial molecules subjected to transient extreme conditions of high pressure, high temperature, and high-strain-rate deformation.[1,5,6] This technique is a unique probe of the large-amplitude high-speed deformation mechanics of molecular structures. As such, it is a useful complement to previous theoretical and experimental studies of monolayer response to slow small-amplitude deformations responsible for the frictional drag of a SAM surface,[10−16] and

the response to slow large-amplitude deformations produced by pushing a probe tip[11,17−27] or an anvil[28−33] into the SAM. The shock compression experiments permit a direct comparison on the relevant time and length scales to atomistic simulations of shock compression,[34] and provide a direct look into the molecular mechanics of many practical applications including molecular lubricants in high-speed engines, molecular lubricants in rifle or cannon barrels, projectile impacts with polymer bulletproof windows and jackets, and high explosives near a detonation front.

SAMs[35] having different molecular structures and molecular packing were studied: the long-chain alkanes octadecanethiol (ODT, $CH_3-(CH_2)_{17}-SH$) or pentadecanethiol (PDT, $CH_3-(CH_2)_{14}-SH$), which terminate in methyl $-CH_3$ groups, and benzyl mercaptan (BMT, $C_6H_5-CH_2-SH$), which terminates in a phenyl group. The effects of zigzag chain structure were investigated by comparing even carbon (C18) ODT and odd carbon (C15) PDT on Au substrates. In both monolayers the all-trans chain-tilt angles are similar, but the terminal methyl groups have small tilt angle ($\theta \approx 23°$) in ODT/Au and large tilt angle ($\theta \approx 60°$) in PDT/Au.[36] The short-chain BMT/Au, which has a minimal number of conformational degrees of freedom, was compared to ODT/Au and PDT/Au, which have a great deal of conformational freedom. ODT/Ag was compared to ODT/Au. On Ag substrates the chains are packed more tightly and are more upright.[37−39]

Planar femtosecond-laser generated shocks with pressures in the Au layer in the 5−10 GPa range were used to compress SAMs.[6] Assuming the hydrocarbon SAMs have physical properties similar to amorphous polyethylene, which has an

* Corresponding author. Ph: (217) 333-3574. E-mail: dlott@scs.uiuc.edu.
† Present address, Institute of Shock Physics, Washington State University, Pullman, WA 99164-2816.

almost identical density of methylene $-CH_2-$ groups,[6] the pressure in the SAM is expected to be in the 0.8 to 1.6 GPa range and the volume compression fraction $\Delta V = (V_i - V_f)/V_i = 0.08-0.13$. The SAMs were anchored to Au or Ag substrates and were covered with an impedance-matched confinement layer of ~1 μm thick ethylene glycol. In uniaxial compression the SAMs are subjected to a combination of compressive and shear stress.[8,40] The shock front had a rise time of <4 ps and a fall time of ~25 ps. The shock velocity was ~3.5 km/s (3.5 nm/ps) and the material velocity was ~0.5 km/s (0.5 nm/ps). The shock causes a cycle of compressive heating and expansive cooling. During an ~20 ps interval of peak shock compression, the peak temperature reaches ~75 °C.[1] After this brief interval when the shock load is released, the temperature returns to within 5-10K of ambient. Measurements were not possible for delay times $t > 1$ ns due to shock-wave breakout and spallation of the sample.

In this paper we will address the following issues:

1. When the shock front arrives, all samples evidence an abrupt (<2.5 ps) loss of C–H stretch SFG signals.[5] A similar SFG signal loss has been observed in static compression experiments on alkanes[28−32] with even numbers of carbon atoms, where the effect was attributed to reorientation or disordering of the methyl terminus or flattening of the molecular axis. It has now been shown[1] that disorder does not cause both the ν_s and ν_{as} CH-stretching transitions of the terminal methyl to vanish, so SFG signal loss must be due to tilting this methyl group to a large angle near 90°. However, the shock experiments do not explain what molecular conformations account for this tilt, nor do they explain why the tilted species did not evidence SFG signals from the adjacent methylene $-CH_2-$ groups that become exposed to the interface with large methyl tilt angles.

2. When the shock unloads, all the SAMs evidence mostly elastic recovery from compression with the prominent exception of ODT/Au. ODT/Au exhibits a clearly viscoelastic response where a significant percentage of the methyl groups remain deformed throughout[6] the ~1 ns observation time. At least two types of deformed molecules are needed to explain the data. One type involves molecules locked in configurations with methyl tilt angles near 90°, which causes them to be SFG invisible. Another type recovers SFG intensity with an ~30 ps time constant, after which they exhibit an enhancement in the ν_s/ν_{as} intensity ratio. This enhanced ratio indicates that some methyl groups have become more upright than the native structure. These differences between odd and even chains are reminiscent of friction-force microscopy experiments[14,41] and dynamic sliding simulations[15,16] that see slightly smaller friction for ODT/Au than PDT/Au, but the shock response is a much more dramatic effect. The experiments alone[1] did not explain why ODT/Au evidenced multiple coexisting species whereas PDT/Au did not.

3. Although the shock responses of PDT/Au, ODT/Ag, and BMT/Au are primarily elastic, there is evidence that shock compression generates 10−20% of the molecules in deformed or defect states. In PDT/Au and ODT/Ag these defects relax back to the native configuration with an ~30 ps time constant whereas in BMT/Au some defects remain up to at least 250 ps.

The structural[42−44] and mechanical[22] properties of alkane SAMs have been extensively reviewed. Quite a few simulations of the equilibrium structures of alkane SAMS on Au(111)[17,21,39,45−54] and of comparisons of Au(111) and Ag(111)[55] have appeared. The structure of BMT has also been studied by simulation.[56]

Simulations and experiment suggest several possible mechanisms for the elastic and viscoelastic response of SAMs under uniaxial compression. Elastic compression occurs when methyl tilt or whole-chain tilting is dominant.[12,14,33] Viscoelastic compression is largely a result of the formation of gauche defects in alkyl chains.[12,17] Gauche defects in all-trans structures result from rotations around carbon–carbon bonds, and lead to shorter fatter chains. Another viscoelastic mechanism that may occur when nanoscopic probe tips are pushed deeply into a SAM is displacement of SAM molecules from their anchor sites,[57] until the probe hits the bare metal surface.[20,22] However, inertial effects preclude SAM displacement from contributing significantly[1] in the shock experiments. It simply takes far to long to move a significant amount of mass away from an ~100 μm diameter spot on the 250 ps time scale of the shock experiments.

In this work we perform several types of calculations. A survey of the SAM energy landscape was performed by looking at a dilute defect, a single distorted SAM molecule surrounded by molecules locked in the native all-trans configuration. Periodic lattices of defect conformers were studied to identify metastable structures that might be generated by shock compression. Several of the most stable of these conformers were studied under conditions of isothermal uniaxial compression. Quasiequilibrium isothermal compression simulations such as these provide a simple, heuristic way of understanding shock compression effects, with the *caveat* that they do not capture all the dynamic features of shock compression.

In our simulations, the SAM lattice is perfect so we do not allow for inhomogeneous sample effects arising, for example, from thermal fluctuations, the domain structure[21,46] and from molecules at domain boundaries. The piston in our theoretical compression apparatus is atomically flat, whereas the shock front emerges from an Au layer with an RMS surface roughness of ~4 nm, which means different segments (shocklets) of the shock front hit the SAM spread over an ~1.3 ps time interval. Nonlinearities arising from the high-strain rate of shock compression are ignored.

2. Methods

These all-atom calculations were performed with the (Cerius[2]) molecular modeling package, with its built-in potential energy parameters.

A. Equilibrium Structures. Supercells of ODT and PDT molecules were constructed in a $(\sqrt{3}\times\sqrt{3})R30°$ lattice on Au-(111).[58] The Au(111) surface was a 3×3 supercell three atomic layers deep. Three thiol molecules were attached at the appropriate locations by Au–S covalent bonds. On the Ag(111) surface, also three atoms deep, the initial supercell was 7×7 and the thiols were in a $(\sqrt{7}\times\sqrt{7})R19.1°$ lattice.[59]

BMT also packs in a $(\sqrt{3}\times\sqrt{3})R30°$ lattice on Au(111),[56] but to accommodate the large terminal benzyl group and the herringbone packing, we used a 6×6 Au(111) supercell with 12 BMT molecules.

B. Single Defect Calculations. A lattice was constructed with a single defect molecule surrounded by two concentric rings of SAM molecules consisting of all nearest and next-nearest neighbors. The dihedral angles of the defect molecule were progressively stepped, and at each step the geometries of the nearest neighbors were varied to minimize the total energy whereas the next-nearest neighbors were held fixed. A limited number of calculations were also performed with three rings of molecules with the outermost ring held fixed. These resulted in no significant changes in the energies of the defect molecule.

Shock Compression of Self-Assembled Monolayers

J. Phys. Chem. B, Vol. 109, No. 11, 2005 **5047**

For PDT and ODT, starting from the all-trans configuration, we systematically varied the dihedral angles of the C−C backbone of the defect molecule. Multiple gauche defects had higher energies than single defects. Deeper defects had higher energies than shallower defects, because larger parts of the chain had to be rotated. On the basis of these energy considerations, we believe it necessary to consider only conformers with either single or double defects located within the first three dihedrals. For single defects, we rotated a dihedral in 10° steps throughout a full 360° whereas the energy was minimized after each step; for double defects we rotated two dihedral angles in 10° steps. With BMT we scanned the dihedral angles of both the −S− CH$_2$ and −CH$_2$−phenyl bonds.

To ensure that no important metastable conformations were missed by these scanning methods, and to gain insights into the population distribution of the different conformers, additional calculations were performed using the Boltzmann jump technique. The lattice was heated to 5000 K to ensure that a wide range of conformations would be sampled, and then the energy was minimized, without the dihedral angle constraints of the previous calculations, to determine the geometries of the individual conformers. These jump methods are similar in spirit to Monte Carlo[25,49] simulations.

C. Defect Lattice Calculations. Using the conformational maps and the results of the Boltzmann jump calculations as a guide, periodic lattices of higher energy metastable conformers were constructed from a single supercell with periodic boundary conditions. Each molecule in the unit supercell was arranged in a specified conformation prior to energy minimization. The energies of these lattices were minimized with only the positions of the Au or Ag atoms constrained. The relative energies and orientations of the molecules were then compared, to each other and to the single-defect results.

D. Uniaxial Isothermal Compression. Uniaxial isothermal compression simulations were performed on periodic lattices of specified molecular conformers. A piston that was a replica of the metal substrate was lowered onto the free surface of the different SAM defect lattices, in 0.2 Å steps for the alkanes and 0.1 Å steps for BMT. The energies of the lattices were minimized at each step. Only the positions of the metal atoms above and beneath the monolayer were constrained.

The compression is characterized by the volume compression factor ΔV,

$$\Delta V = \frac{(V_i - V_f)}{V_i} \tag{1}$$

The estimated pressure[1,6] P_{est} corresponding to each value of ΔV was computed using a Mie-Grüneisen equation of state,[60]

$$P_{est} = -\frac{\partial E}{\partial V} + \Gamma \frac{E}{V} \tag{2}$$

where Γ is the Grüneisen coefficient. In the pressure range being considered, the first term of eq 2 is dominant and the value of P_{est} is not very sensitive to Γ. We used the value[1,6,40] $\Gamma = 1$.

3. Results

A. Equilibrium Structures at Ambient Pressure. In our energy-minimized ODT/Au structure, the molecular chains were tilted from the surface normal by 36.8° and twisted about molecular axis by 49.8°. The ODT/Au methyl tilt (the angle between the methyl C_{3v} axis and surface normal) was 23°. The PDT/Au chain tilt was 35.8°, the twist was 49.4°, and the methyl tilt was 60°. These structures are in excellent agreement with
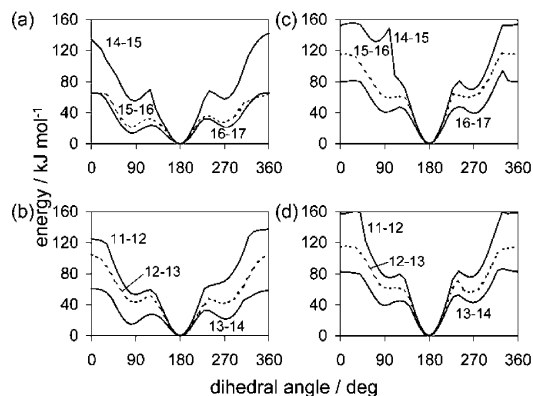

Figure 1. Potential energy surfaces of an individual alkane molecule in an all-trans lattice with rotations around one of the three dihedral angles immediately below the terminal methyl for (a) ODT/Au, (b) PDT/Au, (c) ODT/Ag, and (d) PDT/Ag. The defect energies increase with the number of defects and with the depth of the defects below the terminal methyl, except in ODT/Au where defects at the first and second dihedrals C$_{16-17}$ and C$_{15-16}$ have similar energies.

experiment, especially considering that we did not adjust the potential energy parameters. The consensus experimental chain tilt angle is usually given[42,43] as ∼32°. The measured chain twist[58] on Au is 53°. The methyl tilt angle has been measured[36] by SFG to be 27° for ODT/Au and 58° for PDT/Au. For alkanes on Ag, the energy-minimized chains were nearly upright for both ODT and PDT, with a tilt angle of ∼1° and a methyl tilt of 33°. Experiment[58] gives a chain tilt angle on Ag of ∼10°.

The energy-minimized BMT structure had the −S−CH$_2$−phenyl linkage in the anti configuration, which lets the phenyl rings orient in a low-energy herringbone geometry with rings tilted ∼4° from normal. This is quite close to a previously published model[56] of BMT/Au that used a CHARMM potential modified with electrostatic interaction terms computed using Gaussian 94, which gives this same geometry with a 9° ± 4° tilt.

B. Torsional Landscape of Individual ODT and PDT Defects at Ambient Pressure. We will use the label t for trans, and g for gauche. In this notation, which is greatly simplified from the IUPAC definition, gauche is used as a generic term to indicate a local minimum distinct from trans. The direction of rotation is indicated by a + sign for angles between 0 and 180° or a − sign for angles between 181 and 360° (−179 to 0°). 0° is the cis orientation; 180° is the trans orientation. Because we did not consider the higher energy configurations with defects below the third dihedral, all configurations can be specified using two or three letters; for instance, ttt denotes all-trans, t+gt (or equivalently t+g) denotes a single gauche defect at the second dihedral, and so on.

The computed potential energy functions for individual defect molecules in an otherwise all-trans lattice are shown in Figure 1 for ODT or PDT on Au or Ag. In ODT/Au, single-gauche defects at the first (C$_{16-17}$) or second dihedral (C$_{15-16}$) have similar energies. Deeper defects at the third dihedral and beyond are much higher in energy. In other language, gtt ≈ tgt < ttg < tttg etc. In PDT/Au the energies of single-gauche defects increase monotonically going deeper into the chain, so gtt < tgt < ttg, etc. The small splitting between gtt and tgt in ODT/Au compared to PDT/Au is a consequence of the zigzag chains. Although the energetics of rotating the terminal methyl groups are similar for ODT/Au and PDT/Au, it takes less energy to rotate the two-carbon ethyl group in ODT, which is more upright than the ethyl group in PDT.
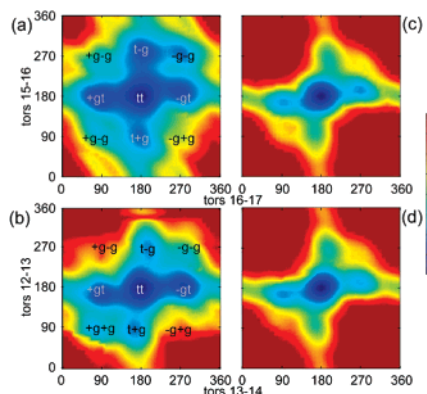
Figure 2. Potential energy surfaces of an individual alkane molecule in an all-trans lattice with rotations around the first two dihedral angles to create either single or double gauche defects, for (a) ODT/Au, (b) PDT/Au, (c) ODT/Ag, and (d) PDT/Ag.

TABLE 1: Conformations and Geometry of Individual Defect Molecules in an All-Trans Lattice of ODT on Au(111)

label	energy (kJ/mol)	16−17 dihedral	15−16 dihedral	14−15 dihedral
ttt	0.00	180°	180°	180°
+gtt	13.14	80.1°	178.2°	−176°
−gtt	17.70	−86.3°	−174.1°	171.3°
t−gt	19.27	−175.9°	−81.2°	−174.4°
t+gt	23.48	177.9°	88.4°	169.4°
−g−gt	29.44	−86.7°	−83.1°	−170.8°
+g+gt	34.87	84.7°	92.2°	164.8°

TABLE 2: Conformations and Geometry of Individual Defect Molecules in an All-Trans Lattice of PDT on Au(111)

label	energy (kJ/mol)	13−14 dihedral	12−13 dihedral	11−12 dihedral
ttt	0.00	180°	179.4°	180°
−gtt	13.67	−82.3°	−175.7°	180°
+gtt	19.98	87.8°	170.9°	180°
t−gt	35.22	−164.6°	−90.9°	−174.2°
t+gt	38.72	165.0°	91.2°	174.3°
+g+gt	42.76	75.5°	88.4°	173.1°

On Ag substrates, the conformational landscapes for ODT and PDT are similar to each other, and the energies of single-gauche defects increase monotonically with depth. The similarity between the ODT/Ag and PDT/Ag landscapes arises because both molecules have minimal ∼0° chain tilts, leading to nearly identical ∼33° methyl tilts.

Figure 2 shows the conformational landscapes for individual defect molecules having single or double gauche on the first two dihedrals. In ODT/Au (Figure 2a) some dual defects including −g−g and +g−g are barely higher in energy than some single defect conformers. The PDT/Au surface in Figure 2b shows a dual-defect +g+g state that is not much higher in energy than t+g and t−g. On Ag substrates, the ODT and PDT surfaces in Figure 2c,d are again quite similar. On Ag the dual defect states are higher in energy than any single-defect state.

The Boltzmann jump technique was used to determine the geometries and energies of the single-molecule defects in the all-trans lattice on Au. Table 1 gives results for ODT/Au and Table 2 gives results for PDT/Au.

C. Torsional Landscapes for Periodic Defect Lattices at Ambient Pressure. Starting with the most stable conformers that emerged from the above analysis, periodic lattices of defects were constructed and energies minimized. The energies and geometries for conformers of ODT/Au and PDT/Au are listed in Tables 3 and 4. It is interesting that in these periodic defect
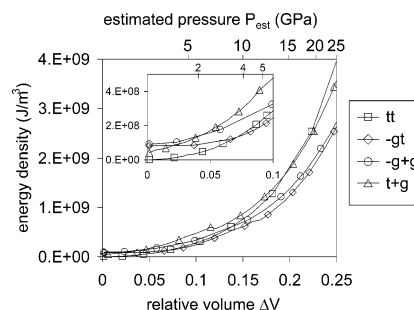

Figure 3. Calculated isothermal planar compression curves for periodic lattices of ODT/Au conformers.

TABLE 3: Conformations and Geometries of Lattices of Periodic ODT Defects on Au(111)

label	energy (kJ/mol)	16−17 dihedral	15−16 dihedral	14−15 dihedral
ttt	0.00	179.8°	179.9°	179.5°
+gtt	16.82	96.1°	179.9°	−175.9°
−gtt	25.58	−97.5°	−164.9°	175.0°
t−g	8.94	−173.6°	−70.9°	−176.6°
t+gt	12.79	178.0°	65.2°	164.4°
−g−gt	23.66	−96.1°	−76.5°	−172.4°
+g+gt	35.40	77.3°	66.7°	147.1°
+g−gt	20.85	100.3°	−78.9°	−174.9°
−g+gt	did not converge			

TABLE 4: Conformations and Geometries of Periodic Lattices of PDT Defects on Au(111)

label	energy (kJ/mol)	13−14 dihedral	12−13 dihedral	11−12 dihedral
ttt	0.00	−179.7°	179.4°	−179.6°
−gtt	6.66	−70.9°	−177.0°	−179.0°
+gtt	12.09	65.2°	164.2°	−177.1°
t−gt	37.85	−171.1°	−103.3°	−164.4°
t+gt	30.84	169.2°	81.6°	−172.8°
+g+gt	29.79	81.0°	100.7°	−178.8°
−g−gt	41.70	−74.1°	−137.4°	−159.8°
+g−gt	did not converge			
−g+gt	did not converge			

models of ODT/Au, the tgt conformers are actually slightly more stable than the gtt conformers, and the +g−g dual defect is almost as stable as the +gt single defect. In PDT/Au, the +g+g dual defect is almost as stable as the tgt conformations, and in fact the energy minimization algorithm often converged on lattices with a mixture of such defects.

In the periodic Ag simulations, there are 21 molecules per supercell, as opposed to merely 3 on Au. Owing to this larger number of molecules, in Ag we often observed mixed states where different conformations coexisted. The individual defect molecule models on Ag (e.g., Figure 2c,d) predicted stable minima for −gt and +gt conformations. However, in the periodic lattice it was impossible to find stable energy-minimized structures for these collective conformations. The most stable configurations appeared to be a mixture of tt and gt states.

D. Torsional Landscapes for BMT/Au at Ambient Pressure. We were unable to find any metastable conformations for BMT at ambient pressure either with single defects or in periodic lattices. The inability to find potential minima away from the equilibrium anti configuration is attributed to the high stability of the herringbone packing of the phenyl rings.

E. Isothermal Compression of ODT/Au and PDT/Au. Figure 3 shows the energies of periodic lattices of ODT/Au conformers under uniaxial isothermal compression. At $\Delta V = 0$ the tt state is most stable, but near $\Delta V = 0.07$ the −gt state becomes more stable. This can be taken to indicate that near
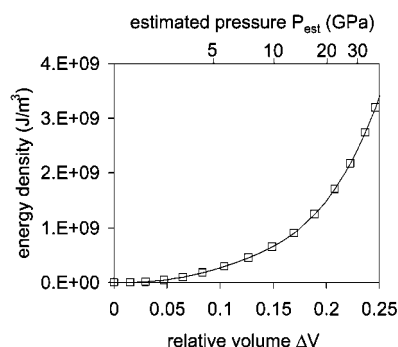
Shock Compression of Self-Assembled Monolayers

J. Phys. Chem. B, Vol. 109, No. 11, 2005 **5049**

Figure 4. Calculated isothermal planar compression curves for periodic lattices of PDT/Au. Only the ttt conformer is stable in this pressure range.
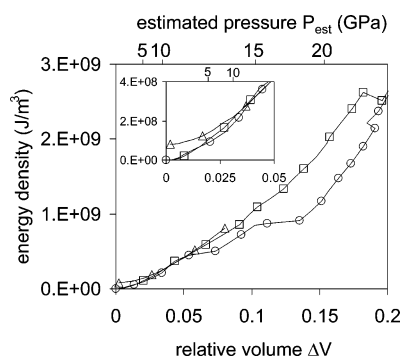

Figure 5. Calculated isothermal planar compression curves for ODT/Ag (□) and PDT/Ag (○). In the $\Delta V = 0.05-0.1$ range, some gauche conformers are observed. A decompression curve for a lattice of mixed ODT/Ag trans and gauche conformers is denoted by (△).

7% compression the all-trans chains lose strength and undergo mechanical failure to create gauche defects. As compression increases there are several state crossings, and in the higher compression regime where $\Delta V > 0.15$, the tt and t+g states are about equally stable. Compression of PDT/Au in Figure 4 is qualitatively different. The tt conformation continues to remain the most stable, even up to 25% compression. Increasing compression merely increases the methyl tilt and the whole-chain tilt.

F. Isothermal Compression of ODT/Ag and PDT/Ag. Alkanes on Ag are packed more densely[37,42] than alkanes on Au, and our study shows the packing on Ag results in lower compressibility. Comparing Figures 3−5 shows that, for instance, a compression factor of $\Delta V = 0.1$ corresponds to an estimated pressure of $P_{est} = 5$ GPa on Au and $P_{est} = 15$ GPa on Ag.

In compression of ODT/Ag, shown in Figure 5, the ttt conformer was most stable. However, in the $\Delta V = 0.05-0.1$ range, mixed states with up to 50% gtt conformers had similar energies. Then with $\Delta V > 0.1$, the pure ttt state was again the most stable. In PDT/Ag, the ttt conformer was dominant, but for $\Delta V > 0.07$ small amounts of gtt conformers began to appear where the compression curve evidences sudden changes in slope.

G. Isothermal Compression of BMT/Au. As shown in Figure 6, BMT/Au in the upright anti configuration has about the same compressibility as ODT/Au. As a periodic lattice of anti molecules was compressed, energy minimization always led to the anti configuration. Attempts to find a stable structure of gauche conformers with phenyl rings near the surface[56] failed until $\Delta V = 0.3$. Then we observed an interesting hysteresis. By decompressing a periodic lattice of gauche conformers, the rings gradually became less tilted but retained the metastable
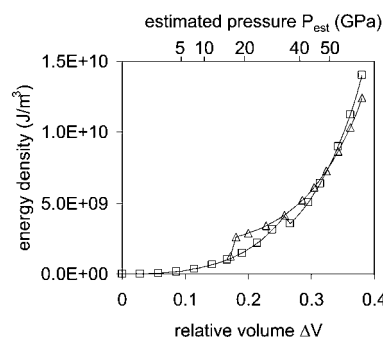

Figure 6. Calculated isothermal planar compression curve for BMT/Au (□) in the native anti configuration. A lattice of gauche conformers was created at $\Delta V = 0.3$. A decompression curve for this lattice, which spontaneously undergoes gauche → anti conversion at $\Delta V \approx 0.15$ is denoted by (△).

gauche conformation until $\Delta V = 0.15$ when the phenyl rings spontaneously returned to the anti state.

H. SFG Susceptibility and Tilt Angle. In the experiments, SFG in the CH stretching region was measured with *ppp* polarization.[1,6] The SFG spectrum of the terminal methyl of the alkanes consists of three resonances denoted[1,61] ν_s, ν_{as} and ν_{FR}. The spectrum of the terminal phenyl consists of a single resonance.[1] These sharper resonances are observed against a broad nonresonant background due to the metal substrate. In static SFG experiments on alkanes, the angular dependence of the ν_s and ν_{as} SFG intensities has been used to establish the absolute orientation of the methyl tilt.[36] In the shock experiments, with foreknowledge of the structure, dynamic changes in these SFG intensities determine the instantaneous methyl tilt angle.[1] The SFG data are presented in the form of a normalized vibrational response function for each resonant CH stretching transition that shows how the signal intensities change relative to the signal from the unshocked native structure. The response function $I(t)$ is defined as[1]

$$I(t) = [I_s(t)/I_{nr}]/[I_{ns}/I_{nr}] \qquad (3)$$

where I_{ns} is the signal intensity with no shock, $I_s(t)$ the signal intensity a delay time t, and I_{nr} is the intensity of the nonresonant signal from the metal layer used as a reference signal to account for changes in laser alignment. The nonresonant signal changes only minimally when the shock arrives.

Measurements of $I(t)$ of alkane SAMs for both ν_s and ν_{as} permit the determination of the instantaneous methyl tilt angle θ, as shown in Figure 7a,b, reproduced from the previous paper.[1] Figure 7a defines the methyl tilt as the angle between the C_{3v} axis and the surface normal. Figure 7b, computed using the methods of Hirose et al.,[62,63] shows how the SFG amplitude changes with tilt angle for the ν_s and ν_{as} CH stretch transitions. It is necessary in this calculation to assume free rotation of the methyl group to determine the ν_{as} result, because ν_{as} is doubly degenerate.[62,63] This assumption is not needed for the ν_s result. Because methyl is quite possibly not a free rotator, especially under compression, the ν_{as} result is regarded as less reliable than the ν_s result. In addition, the ν_s signal strength is generally greater leading to more accurate measurements, so we view fitting the ν_s data as more significant. For the alkane SAMs, Figure 7b shows that with upright methyl groups ($\theta = 0$), the ν_s signal is large and the ν_{as} signal vanishes, whereas with large tilts ($\theta = 90°$) both ν_s and ν_{as} signals vanish.

For BMT, Figure 7c defines the phenyl tilt θ and twist ψ angles. Figure 7d shows the angular dependence of the SFG
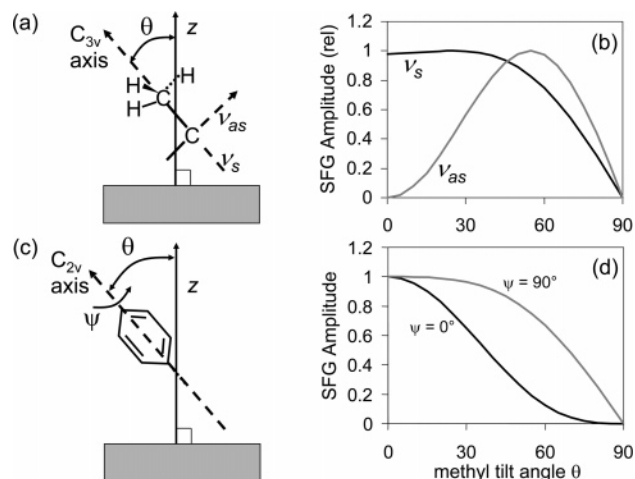
Figure 7. (a) The methyl tilt angle θ for alkanes ODT and PDT is the angle between the surface normal and the methyl C_{3V} axis. (b) Calculated SFG amplitude as a function of tilt angle. (c) The BMT tilt is the angle θ between the phenyl C_{2v} axis and the surface normal. Twist $\psi = 0$ denotes phenyl ring facing the surface, and $\psi = 90°$ denotes phenyl ring on edge. (d) BMT SFG signal amplitudes as a function of tilt angle at two twist angles ψ. Reproduced from ref 1.
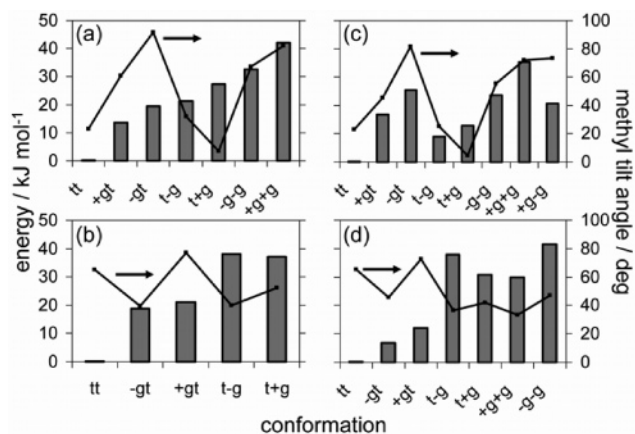

Figure 8. Energies (bars; left axis) and methyl tilt angles (dots; right axis) for alkanes on Au. (a) Energy of a single defect molecule in ODT/Au. (b) Energy of a single defect molecule in PDT/Au. (c) Energy of a defect lattice in ODT/Au. (d) Energy of a defect lattice in PDT/Au. The ODT defects have a larger range of tilt angles than PDT.

signal for the phenyl CH stretch transition. The SFG signal declines monotonically with increasing tilt angle θ. At a given tilt, large twist ($\psi = 90°$) where the ring is on edge relative to the substrate gives larger SFG signals than small twist ($\psi = 0$) where the ring faces the surface.

I. Methyl Tilt Angles for Alkane SAM Conformations on Au. Figure 8 shows the methyl tilt angles for ODT/Au and PDT/Au for conformers with 0, 1, or 2 gauche defects at the first two dihedrals. Shown in the figure are all the conformers that have local minima at ambient pressure. The left two panels refer to individual defect molecules and the right two panels to periodic defect lattices. In ODT/Au there is a greater diversity of tilt angles than in PDT/Au. It will be significant to note that the ODT/Au −gt and +g+g have large tilts and that t+g is nearly upright. The conformer energies are different in the single-defect and periodic lattice models. Because the individual defect and periodic lattice models are fundamentally different, direct comparisons between the energies of particular conformations in the two models is not possible.

Figure 9 shows the structures of some of the conformers of PDT/Au and ODT/Au under compression needed to understand

the shock experiments. With PDT/Au under uniaxial stress, the ttt conformer is always the most stable. Compression increases the methyl tilt and the whole-chain tilt, giving methyl tilt angles that range from 65° at ambient pressure to 80° at $\Delta V = 28\%$, as shown in Figure 9a,b.

With ODT/Au in Figure 9c, look closely at the ttt, −gtt, and +gtt conformers. Because of the initial tilt of the ttt conformation, compressing the SAM with a piston from above tilts the methyl group toward the −g direction and away from the +g direction. Although −gtt and +gtt conformations are energetically similar, the dynamics of shock compression selectively generates the −g conformations. Thus the single and double gauche configurations that can be generated by shock compression of ODT/Au are −gtt and −g+gt shown in Figure 9c. Both of these conformers have high methyl tilt angles near 85°. In the experiments, post-shock ODT/Au evidences a species with a nearly upright methyl tilt. The t+gt conformer shown in Figure 9c fits this description, having a tilt angle of 12°.

4. Discussion and Comparison to Experiment

The most dramatic effect seen by experiment is the difference between the nearly elastic recovery of PDT even chains and the viscoelastic recovery of ODT odd chains on Au substrates. In this section we will use input from the simulation results to fit these experimental data. The PDT/Au, ODT/Ag, and BMT/Au SAMs evidence mainly elastic recovery but do show a small degree, 10−20%, of viscoelastic recovery. Our simulations results will in these cases be used to comment on possible mechanisms of molecular deformation.

A. PDT/Au. The isothermal compression simulations show that compression increases the PDT/Au methyl tilt angle only, so fitting the elastic recovery in the data is a straightforward problem requiring only the temporal envelope of the shock $f(t)$, the ΔV-dependent tilt angle $\theta(\Delta V)$, and the tilt-angle dependent SFG intensity $I(\theta)$. The temporal envelope of the shock can be fit to a phenomenological function of the form[1]

$$f(t) = (1 + \exp[-(t - t_0)/t_r] + \exp[(t - t_0)/t_f])^{-1} \quad (4)$$

where the constants $t_r = 1.1$ ps and $t_f = 9.6$ ps are obtained by fitting the observed rise and fall times (10% to 90%) of 4 and 25 ps, respectively, and t_0 indicates the arrival time of the shock front at the SAM. In the experiments, a vibrational response function is measured, which drops from 1 to 0. To compare the vibrational response function to eq 4, we compare the experimental data to the function $1 - f(t)/f_{max}(t)$, where $f_{max}(t)$ is the maximum value of $f(t)$. The shock-generating laser pulse arrival is defined[5] as $t = 0$, and the shock arrival at the SAM occurs at $t_0 \approx 50$ ps. We assume a linear relationship between the shock compression envelope and ΔV which is valid for small ΔV,

$$\Delta V(t) = \Delta V_{max} f(t) \quad (5)$$

where ΔV_{max} is the value of ΔV at maximum compression, $\Delta V_{max} \approx 0.13$ for ODT and PDT/Au. For the less compressible ODT/Ag, ΔV_{max} is about one-half this value. When we compute the PDT/Au methyl tilt angle versus ΔV, we find the tilt angle increases approximately linearly from 65° to 78° as ΔV increases from 0 to 0.25. Combining this result with $I(\theta)$ data from Figure 7b, we determine the time-dependent vibrational response function. The comparison with experimental data for ν_s and ν_{as} from ref 1 is shown in Figure 10a,b.

Our fit to the PDT/Au data in Figure 10a,b does not have enough SFG signal loss at the shock maximum. The observed signal loss is ~90%, which is consistent with a PDT methyl
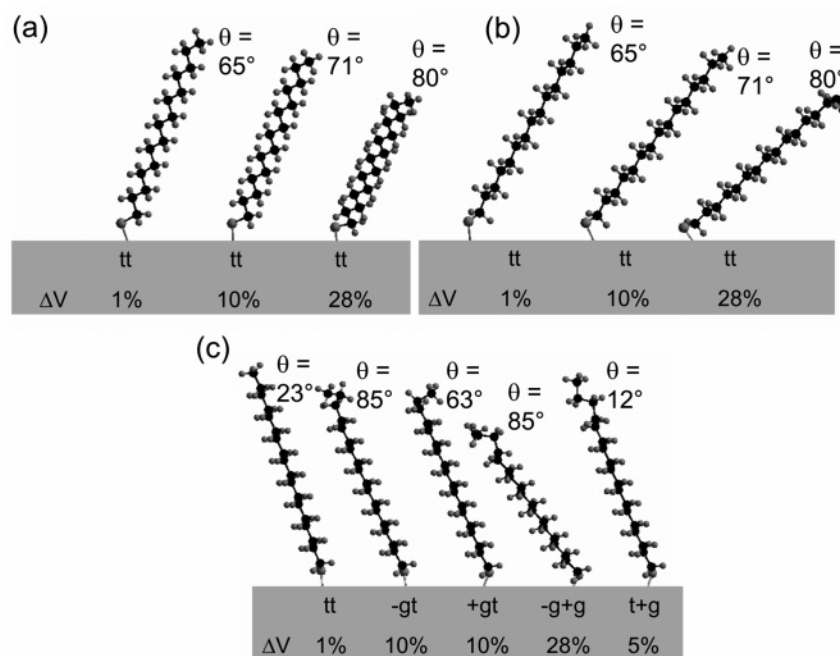
Shock Compression of Self-Assembled Monolayers

J. Phys. Chem. B, Vol. 109, No. 11, 2005 **5051**

Figure 9. Models of PDT/Au and ODT/Au conformers and their methyl tilt angles θ that are used to fit the shock compression data, at indicated values of the compression ΔV. (a) and (b) views of PDT molecules from two perspectives. With increasing compression the ttt conformer remains dominant but the methyl and whole-chain tilt increases. (c) ODT shock compression creates defects with the first dihedral in the $-g$ state. The $+g$ conformer tilts in the wrong direction to be created by a planar compression. The shock can create single $-gtt$ and double $-g+gt$ conformers with high tilt angles that are nearly SFG-invisible. The $-g+gt$ conformer at ambient pressure has no discernible energy barrier to transform into the nearly upright t+gt state.
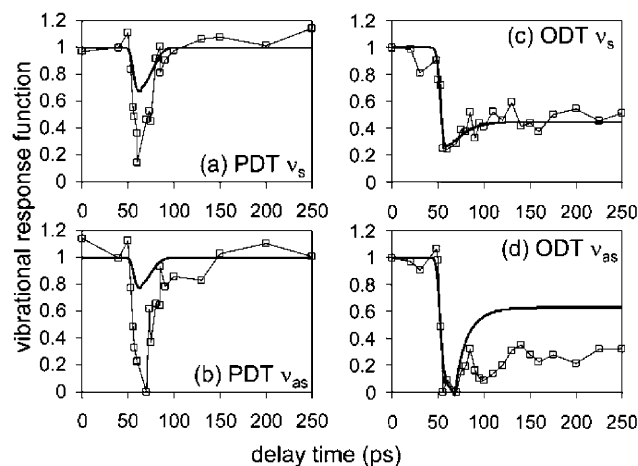

Figure 10. Computed fits to shock compression data ($\square$) from ref 1. The PDT fits for ν_s and ν_{as} underestimate the observed SFG signal loss. The ODT fit is excellent for ν_s but it overestimates the ν_{as} signal at longer delay times.

tilt of $\sim85°$. However, at $\Delta V = 0.1$, the calculated tilt angle under isothermal compression is $\sim75°$. Thus our calculations somewhat underestimate the shock-induced methyl tilt angle.

B. ODT/Au. To explain the rather complicated ODT/Au shock response requires that the shock create, directly or indirectly, at least three different species. The shock must create two kinds of SFG-invisible conformers. One must remain invisible for times $t > 250$ ps to explain the long-time signal loss. The other must decay in ~30 ps into a nearly upright species to explain the enhanced ν_s/ν_{as} signal ratio.

Figure 3 indicates that with $\Delta V = 0.13$ in ODT/Au, most single- and double-gauche defect states have similar energies. But shock dynamics favor defects with $-g$ at the first dihedral, so we propose that a shock could create a mixture of $-gt$ and $-g+g$ conformers. Parts a and b of Figure 8 show that both of

these conformers are nearly SFG-invisible, with methyl tilts of $\sim85°$. When the shock unloads, both conformers are unstable to relaxation back to tt. The ambient pressure potential surface in Figure 2a shows there is a barrier for $-gt$ to relax back to tt, so $-gt$ could be kinetically trapped in an SFG-invisible state on the experimental time scale of 250 ps. The $-g+g$ conformer has a similar barrier to tt, but there is no barrier for $-g+g \rightarrow$ t+g isomerization. The t+g state is metastable, having a barrier to t+g $\rightarrow$ tt relaxation, and its geometry is nearly upright, with a methyl tilt of $\theta = 12°$. Thus the ODT/Au data are fit with the scheme[6]

$$ttt \xrightarrow{\text{shock}} -gtt + -g+gt$$

$$-g+gt \xrightarrow[\sim 30 \text{ ps}]{\text{unloading}} t+gt$$
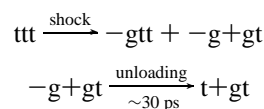
Our compression simulations do not determine the relative abundances of single and double-defect states behind the shock front, but this information can be extracted to some degree by fitting the ODT/Au data for ν_s. The results are shown in Figure 11, where the shock during its ~4 ps rise creates an approximately 75:25 mixture of single gauche $-gt$ conformers and double gauche $-g+g$ conformers. All the $-g+g$ conformers subsequently relax into t+g. However, because both $-gt$ and $-g+g$ are not observed by SFG, this fit to the data is not unique; a more complicated model exists where the labile $-g+gt$ conformer is created in greater abundance and then allowed to generate *both* $-gtt$ and t+gt. An example of one of these more complicated fits is also shown in Figure 11 as dashed curves. The solid curves in Figure 11 were convolved with the shock front fall time and the results were used to fit the data in Figure 10c,d. The ν_s fit is excellent, whereas the ν_{as} fit somewhat overpredicts the long-time ν_{as} signal level. However, as explained in section 3H, we believe our predictions of the ν_s hyperpolarizability are more accurate than for ν_{as}.
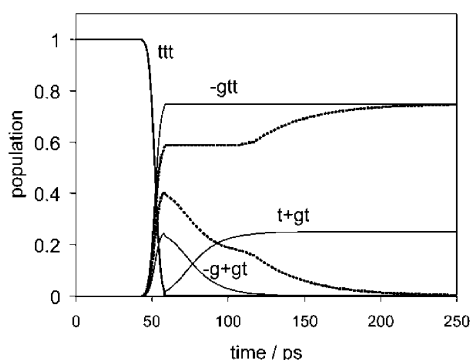
Figure 11. Time dependent populations of ODT/Au conformers used to fit the data in Figure 10c,d. The shock in ~4 ps produces an ~75:25 mixture of −gtt and −g+gt single and double gauche defects. As the shock unloads, the −g+gt conformer converts to more upright t+gt with an ~30 ps time constant. Alternative fits (dotted lines) have the shock creating more of the double-defect −g+gt conformer, which is allowed to convert into both t+gt and −gtt with an ~30 ps time constant.

The molecular models of the single and double gauche defect conformers in Figure 9c also explain why we do not see methylene SFG transitions in the spectrum of shocked alkanes. Methylene transitions are similarly not seen in static compression experiments.[28−32] In an ordered all-trans lattice, methylene groups are in a nearly centrosymmetric environment that cannot be seen with SFG, but with a mixture of ODT defect conformers one might expect to see broken symmetry leading to observable transitions from the methylene at C17. However, in the −gtt, −g+gt and t+gt structures, the bisector of the H−C−H angle of C17, which is parallel to the transition moment, lies nearly parallel to the metal surface. This orientation results in negligible ppp SFG intensity, because the parallel electric field vanishes at the metallic surface.

C. SAM Compressibilities. In Figures 3−6 we plotted the SAM energies as a function of ΔV. Along with ΔV we provided values of P_{est} calculated using eq 2. The isothermal compressibility can be extracted from the limiting slope of P vs ΔV as $\Delta V \rightarrow 0$. Figures 3, 4, and 6 show that all the SAMs on Au have similar compressibilities. The compression factor $\Delta V = 0.1$ at about 5 GPa. The SAMs on Ag in Figure 5 are about a factor of 3 less compressible, because $\Delta V = 0.1$ at about 15 GPa.

Although we believe our *comparative* compressibilities are reasonable, our SAM models appear to be less compressible than what has been found in other simulations. Henda[33] sees $\Delta V = 0.1$ at 2.5 GPa, and Siepmann and McDonald[25] obtain similar results. It is known that the compressibility[33] is quite sensitive to the potential and we did not optimize our potential as these other authors did, so we believe our estimated pressures are overstated by a factor of ~2−3.

D. Viscoelasticity of PDT/Au, ODT/Ag, and BMT/Au. Figure 12 shows data taken from ref 1 that illustrate the minor viscoelastic contributions to the unloading process in PDT/Au, ODT/Ag and BMT/Au. Immediately after the shock finishes unloading (near $t = 85$ ps), all three SAMs evidence an ~30 ps process. With PDT/Au and ODT/Ag this process leads to complete recovery of the SFG signal, but with BMT/Au signal recovery is not quite complete even up to 250 ps scale.

In PDT/Au (Figure 10a,b), immediately after the shock unloads the delayed recovery of the ν_{as} signal means that the ν_s/ν_{as} ratio is temporarily enhanced relative to the native structure. This suggests that the shock front, in addition to simple methyl tilting, also creates a minor population of defect states
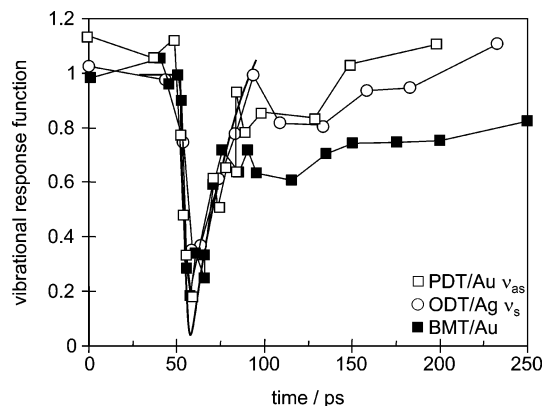

Figure 12. Experimental data for ν_{as} of shocked PDT/Au, ν_s of ODT/Ag and phenyl CH stretch of BMT/Au, reproduced from ref 1. The heavy solid curve denotes the shock compression temporal envelope. These SAMs show mostly elastic recovery from shock with a small contribution from viscoelasticity.

that evidence an enhanced ν_s/ν_{as} ratio. In other words, to fit the data, we must postulate that the actual shock front creates more defects than we see in our isothermal compression simulations. When the shock unloads, these defects become metastable and relax back to the all-trans structure. There are not enough data to uniquely determine the defect concentration and the tilt angle. Figure 7b shows that conformers with methyl tilts <40° give about the same ν_s intensity as the all-trans structure but less ν_{as} intensity. Figure 8d shows that several conformers have the needed tilt angle, with the −gt conformer seemingly the most reasonable choice based on its appearance in our isothermal compression simulations.

The isothermal compression simulations do not do a good job of explaining the shock-induced SFG signal loss in ODT/Ag and BMT/Au in a quantitative manner but they are suggestive of the basic molecular mechanisms behind signal loss and the small amount of viscoelastic recovery. The computed volume compression factors and estimated pressures needed for large methyl tilts in ODT/Ag or large phenyl tilts via anti-to-gauche isomerization in BMT/Au considerably exceed the values used in experiment. This observation again suggests the isothermal compression simulations underestimate the effects of dynamic shock compression. The simulations do suggest that in ODT/Au, the main features of the SFG signal are caused by methyl tilting and elastic recovery. The minor viscoelastic component in the ODT/Ag data in Figure 12 seems most likely to result from a small population of −gt conformers, which are observed in Figure 5 when $\Delta V > 0.05$.

In BMT/Au, if we assume that the shock is able to create SFG-invisible gauche conformers of BMT, our simulations still do not explain the small component of long-term SFG signal loss in BMT/Au, because simulations see no metastable BMT conformers at ambient pressure. This leads us to speculate the long-term signal loss is due to BMT molecules at domain boundaries or at surface defects. A possible interpretation for the ~30 ps transient in the BMT data is suggested by Figure 7d. It might involve twisting motions of BMT molecules trapped in high-tilt states.

5. Conclusions

The molecular simulations do a good job of suggesting which molecular conformations could give rise to the observed SFG signals, and through determining the tilt angles, the simulations determine relative changes in the molecular hyperpolarizability needed to fit the time-dependent SFG data. The simulations

Shock Compression of Self-Assembled Monolayers

J. Phys. Chem. B, Vol. 109, No. 11, 2005 **5053**

provide input that leads to good fits to the ODT/Au and PDT/Au data, except that the predicted SFG signal loss is somewhat smaller than in experiment. The simulations greatly underpredict SFG signal loss for ODT/Ag and BMT/Au.

It is clear that the isothermal compression simulations systematically underestimate the ability of the shock front to create defects. This is of course not a surprise, because shock compression is a much more violent and nonlinear perturbation than isothermal compression. Broadly speaking, there are four reasons why shock compression could be expected to create many more defects than slow isothermal compression. (1) During the shock lasting a few tens of picoseconds, although the SAM anchor is cold, the methyl or phenyl groups are in contact with a shock-heated fluid at a temperature of ~75 °C. (2) The large-strain-rate facilitates barrier crossings to a greater degree than slow compression by greatly reducing the effective viscosity of the SAM. The directed energy of the shock can be more effective in helping a system surmount barriers if the configurational coordinate has a significant component along the direction of shock propagation. In picosecond laser-driven shock compression experiments on polymers and proteins, Kim et al.[7,8] have seen effective viscosities under shock compression that are orders of magnitude less than what is measured in low-strain-rate experiments (3) The SAM substrates have 4 nm RMS roughness,[1] the SAMs have a complicated domain structure and they evidence finite-temperature disordering, which are features not included in our small-scale simulations.[38,46] Compression-induced defect formation may be much easier in valleys and ridges, at domain boundaries or in locally disordered regions. (4) The shock front has inhomogeneities also not present in our simulations. The front has a roughness similar to the ~4 nm RMS roughness of the metal substrate. The leading elements of the shock front (shocklets[64]) compress regions of the SAM surrounded by undisturbed material. When the trailing shocklets arrive, they compress regions that are experiencing shear forces from the surrounding already-compressed material, which might make them easier to tilt and twist.

Even though the isothermal compression approach underestimates the effects of the shock front, it does provide a convincing explanation for the dramatically different behaviors of PDT/Au and ODT/Au. Although both SAMS have similar compressibilities, the PDT/Au compresses by elastic tilting and the ODT/Au compresses by gauche defect formation. In ODT/Au both single and double defects are similar in energy, leading to a mixture of conformers. Because both SAMs are in the long-chain limit (more than 10–12 carbon atoms[42]), where increased chain length has little effect on the binding energy per carbon atom, the differences between the two stems mostly from the zigzag nature of even and odd chains. The greater methyl tilt in PDT/Au creates higher barriers to chain twisting needed to generate gauche defects.

References and Notes

(1) Lagutchev, A. S.; Patterson, J. E.; Huang, W.; Dlott, D. D. *J. Phys. Chem. B* **2005**, *109*, 5033.
(2) Zhu, X. D.; Suhr, H.; Shen, Y. R. *Phys. Rev. B* **1987**, *35*, 3047.
(3) Harris, A. L.; Chidsey, C. E. D.; Levinos, N. J.; Loiacono, D. N. *Chem. Phys. Lett.* **1987**, *141*, 350.
(4) Bain, C. D. *J. Chem. Soc., Faraday Trans.* **1995**, *91*, 1281.
(5) Patterson, J.; Lagutchev, A. S.; Dlott, D. D. *AIP Conf. Proc.* **2004**, *706*, 1299.
(6) Patterson, J.; Lagutchev, A. S.; Huang, W.; Dlott, D. D. *Phys. Rev. Lett.*, in press.
(7) Kim, H.; Hambir, S. A.; Dlott, D. D. *Phys. Rev. Lett.* **1999**, *83*, 5034.
(8) Kim, H.; Hambir, S. A.; Dlott, D. D. *J. Phys. Chem. B* **2000**, *104*, 4239.
(9) Graham, R. A. *Solids Under High-Pressure Shock Compression. Mechanics, Physics and Chemistry*; Springer-Verlag: New York, 1993.
(10) Harrison, J. A.; White, C. T.; Colton, R. J.; Brenner, D. W. *J. Phys. Chem.* **1993**, *97*, 3.
(11) Zhang, S.; Lan, H. *Tribol. Int.* **2002**, *35*, 321.
(12) Brewer, N. J.; Foster, T. T.; Leggett, G. J.; Alexander, M. R.; McAlpine, E. *J. Phys. Chem. B* **2004**, *108*, 4723.
(13) Rai, B.; Sathish, P.; Malhotra, C. P.; Pradip; Ayappa, K. G. *Langmuir* **2004**, *20*, 3138.
(14) Wong, S.-S.; Takano, H.; Porter, M. D. *Anal. Chem.* **1998**, *70*, 5209.
(15) Mikulski, P. T.; Harrison, J. A. *Tribol. Lett.* **2001**, *10*, 29.
(16) Mikulski, P. T.; Harrison, J. A. *J. Am. Chem. Soc.* **2002**, *123*, 6873.
(17) Barrena, E.; Ocal, C.; Salmeron, M. *J. Chem. Phys.* **2000**, *113*, 2413.
(18) Salmeron, M. *Tribol. Lett.* **2001**, *10*, 69.
(19) Salmeron, M.; Neubauer, G.; Folch, A.; Tomitori, M.; Ogletree, D. F.; Sautet, P. *Langmuir* **1993**, *9*, 3600.
(20) Liu, G.; Salmeron, M. B. *Langmuir* **1994**, *10*, 367.
(21) Li, B.; Zeng, C.; Li, Q.; Wang, B.; Yuan, L.; Wang, H.; Yang, J.; Hou, J. G.; Zhu, Q. *J. Phys. Chem. B* **2003**, *107*, 972.
(22) Carpick, R. W.; Salmeron, M. *Chem. Rev.* **1997**, *97*, 1163.
(23) Bonner, T.; Baratoff, A. *Surf. Sci.* **1997**, *377–379*, 1082.
(24) Siepmann, J. I. *Tribol. Lett.* **1995**, *1*, 191.
(25) Siepmann, J. I.; McDonald, I. R. *Phys. Rev. Lett.* **1993**, *70*, 453.
(26) Tupper, K. J.; Brenner, D. W. *Langmuir* **1994**, *10*, 2335.
(27) Tupper, K. J.; Colton, R. J.; Brenner, D. W. *Langmuir* **1994**, *10*, 2041.
(28) Du, Q.; Xiao, X.-D.; Charych, D.; Wolf, F.; Frantz, P.; Shen, Y. R.; Salmeron, M. *Phys. Rev. B* **1995**, *51*, 7456.
(29) Fraenkel, R.; Butterworth, G. E.; Bain, C. D. *J. Am. Chem. Soc.* **1998**, *120*, 203.
(30) Beattie, D. A.; Haydock, S.; Bain, C. D. *Vibr. Spectrosc.* **2000**, *24*, 109.
(31) Berg, O.; Klenerman, D. *J. Appl. Phys.* **2001**, *90*, 5070.
(32) Berg, O.; Klenerman, D. *J. Am. Chem. Soc.* **2003**, *125*, 5493.
(33) Henda, R. *AIChE J.* **2000**, *46*, 1275.
(34) Holian, B. L. *Shock Waves* **2004**, *13*, 489.
(35) Bain, C. D.; Troughton, E. B.; Tao, Y.-T.; Evall, J.; Whitesides, G. M.; Nuzzo, R. G. *J. Am. Chem. Soc.* **1989**, *111*, 321.
(36) Nishi, N.; Hobara, D.; Yamamoto, M.; Kakiuchi, T. *J. Chem. Phys.* **2003**, *118*, 1904.
(37) Laibinis, P. E.; Whitesides, G. M.; Allara, D. L.; Tao, Y. T.; An, P.; Nuzzo, R. G. *J. Am. Chem. Soc.* **1991**, *113*, 7152.
(38) Vemparala, S.; Karki, B. B.; Kalia, R. K.; Nakano, A.; Vashishta, P. *J. Chem. Phys.* **2004**, *121*, 4323.
(39) Bareman, J. P.; Klein, M. L. *J. Phys. Chem.* **1990**, *94*, 5202.
(40) Zel'dovich, Y. B.; Raiser, Y. P. *Physics of Shock Waves and High-temperature Hydrodynamic Phenomena*; Academic Press: New York, 1966.
(41) Lee, S.; Shon, Y.-S.; Colorado, J. R.; Guenard, R. L.; Lee, T. R.; Perry, S. S. *Langmuir* **2000**, *16*, 2220.
(42) Schreiber, F. *Prog. Surf. Sci.* **2000**, *65*, 151.
(43) Dubois, L. H.; Nuzzo, R. G. *Annu. Rev. Phys. Chem.* **1992**, *43*, 437.
(44) Jiang, S. *Mol. Phys.* **2000**, *100*, 2261
(45) Ulman, A.; Eilers, J. E.; Tillman, N. *Langmuir* **1989**, *5*, 1147.
(46) Siepmann, J. I.; McDonald, I. R. *Langmuir* **1993**, *9*, 2351.
(47) Hautman, J.; Klein, M. L. *J. Chem. Phys.* **1989**, *91*, 4994.
(48) Hautman, J.; Bareman, J. P.; Mar, W.; Klein, M. L. *J. Chem. Soc., Faraday Trans* **1991**, *87*, 2031.
(49) Balasubramanian, S.; Klein, M. L.; Siepmann, J. I. *J. Chem. Phys.* **1995**, *103*, 3184.

(50) Gronbech-Jensen, N.; Parikh, A. N.; Beardmore, K. M.; Desai, R. C. *Langmuir* **2003**, *19*, 1474.

(51) Li, T.-W.; Chao, I.; Tao, Y.-T. *J. Phys. Chem. B* **1998**, *102*, 2935.

(52) Tachibana, M.; Yoshizawa, K.; Ogawa, A.; Fujimoto, H.; Hoffmann, R. *J. Phys. Chem. B* **2002**, *106*, 12727.

(53) Shevade, A. V.; Zhou, J.; Zin, M. T.; Jiang, S. *Langmuir* **2001**, *17*, 7566.

(54) Mar, W.; Klein, M. L. *Langmuir* **1994**, *10*, 188.

(55) Sellers, H. A.; Ulman, A.; Shnidman, Y.; Eilers, J. E. *J. Am. Chem. Soc.* **1993**, *115*, 9389.

(56) Jung, H. H.; Won, Y. D.; Shin, S.; Kim, K. *Langmuir* **1999**, *15*, 1147.

(57) Joyce, S. A.; Thomas, R. C.; Houston, J. E.; Michalske, T. A.; Crooks, R. M. *Phys. Rev. Lett.* **1992**, *68*, 2790.

(58) Bensebaa, F.; Ellis, T. H.; Badia, A.; Lennox, R. B. *Langmuir* **1998**, *14*, 2361.

(59) Rieley, H.; Kendall, G. K. *Langmuir* **1999**, *15*, 8867.

(60) Ashcroft, N. W.; Mermin, N. D. *Solid State Physics*; Holt, Reinhart and Winston: New York, 1976.

(61) Richter, L. J.; Petralli-Mallow, T. P.; Stephenson, J. P. *Opt. Lett.* **1998**, *23*, 1594.

(62) Hirose, C.; Akamatsu, N.; Domen, K. *J. Chem. Phys.* **1992**, *96*, 997.

(63) Hirose, C.; Akamatsu, N.; Domen, K. *Appl. Spectrosc.* **1992**, *46*, 1051.

(64) Hambir, S. A.; Kim, H.; Dlott, D. D.; Frey, R. B. *J. Appl. Phys.* **2001**, *90*, 5139.